

Engineered Self-Organization for Resilient Robot Self-Assembly with Minimal Surprise

Tanja Katharina Kaiser and Heiko Hamann

Institute of Computer Engineering, University of Lübeck, Germany

Abstract

In collective robotic systems, the automatic generation of controllers for complex tasks is still a challenging problem. Open-ended evolution of complex robot behaviors can be a possible solution whereby an intrinsic driver for pattern formation and self-organization may prove to be important. We implement such a driver in collective robot systems by evolving prediction networks as world models in pair with action-selection networks. Fitness is given for good predictions which causes a bias towards easily predictable environments and behaviors in the form of emergent patterns, that is, environments of minimal surprise. There is no task-dependent bias or any other explicit predetermination for the different qualities of the emerging patterns. A careful configuration of actions, sensor models, and the environment is required to stimulate the emergence of complex behaviors. We study self-assembly to increase the scenario's complexity for our minimal surprise approach and, at the same time, limit the complexity of our simulations to a grid world to manage the feasibility of this approach. We investigate the impact of different swarm densities and the shape of the environment on the emergent patterns. Furthermore, we study how evolution can be biased towards the emergence of desired patterns. We analyze the resilience of the resulting self-assembly behaviors by causing damages to the assembled pattern and observe the self-organized self-repair process. In summary, we evolved swarm behaviors for resilient self-assembly and successfully engineered self-organization in simulation. In future work, we plan to transfer our approach to a swarm of real robots.

Keywords: self-assembly, evolutionary swarm robotics, pattern formation, self-organization

1. Introduction

In swarm robotics self-organizing robots collaborate to complete tasks [1, 2]. As each robot acts autonomously and relies on local information only, the robot

Email address: {kaiser, hamann}@iti.uni-luebeck.de (Tanja Katharina Kaiser and Heiko Hamann)

swarm forms a decentralized system. The manual design of decentralized systems is known to be difficult [3, 1]. Methods of machine learning, such as multi-agent learning [4, 5], seem a reasonable option. However, the automatic generation of robot controllers for complex tasks and even more for collective robot systems is still challenging [6], despite recent improvements in machine learning [7, 8]. An additional challenge is, how the decentralized system may be able to improve its performance at runtime, stay adaptive to changes in the environment, and increase its own capabilities and complexity. A possible solution can be the implementation of open-ended evolution [9, 10] of robot behaviors that may generate more and more complex, task-independent, and interesting behaviors by itself [11, 12]. Applying methods of evolutionary robotics to swarm robotics is evolutionary swarm robotics [3]. However, especially the design of fitness functions remains challenging in evolutionary robotics [13]. While a priori domain-specific knowledge influences the outcome and performance positively, it foils the idea of evolution as a black-box optimizer at the same time [14, 15]. Furthermore, the fitness function has to be designed carefully such that the evolutionary algorithm does not converge prematurely [16].

The creation of an intrinsic driver for pattern formation and self-organization may be a potential strategy to overcome these challenges. A built-in implicit motivation for forming patterns instead of task-specific rewards may have more potential to create complex robot behaviors. We are loosely inspired by Friston’s work on a free-energy principle for natural brains in search for such a driver [17]. Friston assumes that vertebrates have an innate driver to minimize surprise as brains continually try to predict their environment. Organisms may have a tendency to stay in safe and boring environments meaning that the organism’s brain can easily predict them and thus, an evolutionary advantage arises. We roughly follow this concept by making the innate driver explicit as selective pressure on making good predictions in our work [18, 19, 20]. We evolve pairs of artificial neural networks (ANN) whereby one serves as a typical robot controller. The other ANN serves as a world model which predicts the next sensor values based on the currently observed values and represents a model of the robot’s environment. We only observed four basic swarm behaviors in our previous studies in 1D and 2D continuous simulation environments. To move to the next level of complexity, we study self-assembly. At the same time, we limit ourselves to a 2D grid world to ensure the feasibility of our study which leads to a simplification of sensing and equidistant positioning of robots. Our objective will be to exploit this paper’s results from grid-based simulations and transfer them to robots, although this will be challenging.

This paper extends our previous work [21] by a comparison of different sensor models for the use in our self-assembly scenario as well as by a study of the resilience of the emergent self-assembly behaviors. We introduce our minimal surprise approach in Sect. 1.1 and present related work in Sec. 1.2. Section 2 presents methods ranging from the setup for evolving self-assembly behaviors with minimal surprise (Sec. 2.1) over metrics for structure classification (Sec. 2.2) up to the selection of the sensor model (Sec. 2.3). We present our results in Sec. 3. In Sec. 3.1, we show evolved self-assembly behaviors in differ-

ent swarm densities and engineer self-organized self-assembly in Sec. 3.2. The resilience of the evolved behaviors is illustrated in Sec. 3.3. Section 4 discusses our results and outlines future work.

1.1. The Minimal Surprise Approach

Using minimal surprise, we aim for the emergence of swarm behaviors ranging from simple behaviors like aggregation to more complex behaviors like self-assembly. Our robot swarms of size N lived on simulated 1D and 2D torus environments so far, but we aim for the extension to real world scenarios in future work [18, 19]. Each swarm member (robot), is equipped with a pair of three-layered ANNs that are evolved jointly. A regular controller is implemented by a feedforward network, that we call action network (see Fig. 1a). One output of the action network represents the robot’s next action, which is either straight motion or rotation, and there may be additional outputs depending on the experimental setting.

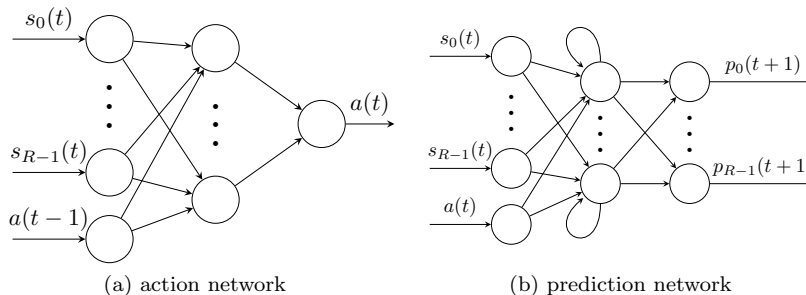


Figure 1: ANN pair of each robot. $a(t - 1)$ is the robot’s last action value and $a(t)$ is its next action. $s_0(t), \dots, s_{R-1}(t)$ are the R sensor values of the robot at time step t , $p_0(t + 1), \dots, p_{R-1}(t + 1)$ are its sensor value predictions for time step $t + 1$. Adapted by permission from Springer Nature Customer Service Centre GmbH: [21], ©Springer Nature Switzerland AG 2019.

Additionally, the prediction network (see Fig. 1b), that is implemented as a recurrent network, enables robots to predict their sensor values of the next time step. As each robot uses exteroceptive sensors, the prediction network predicts each robot’s environment and thus, is a world model. The current sensor values of a robot are given as inputs to both networks. The robot’s last action value is given as an additional input to the action network while the next action is given to the prediction network. The prediction network might thus be enabled to make better predictions as it receives additional information about the next time step.

We apply a simple genetic algorithm [22]. The genomes are randomly generated for the initial population and consist of two sets of weights, one for the action network and one for the prediction network. We have exclusively homogeneous swarms as all robots of an evaluation have instances of the same ANN

pair, that is, they share the same genome. Thus, we have two concepts of populations: a population of genomes encoding pairs of ANN for the evolutionary algorithm and a population of robots forming a homogeneous swarm used in the evaluations of a genome. We use discrete sensors in all experiments. The sensors output a ‘1’ if another robot is detected and a ‘0’ otherwise. We reward good predictions, that is, we put selective pressure on the prediction network while the action network is not directly rewarded. Thus, the action network receives no direct selective pressure, but is subject to genetic drift. As action networks and prediction networks are evaluated collectively as pairs, high fitness values can only be reached if the selected actions of the action network lead to behaviors that fit to the sensor value predictions of the prediction network. ANN pairs which receive high fitness values have a higher likelihood to survive in the evolutionary process and consequently, the action network receives indirect selective pressure.

The fitness function rewards correct predictions with a fitness value normalized to a maximum of 1. We define the fitness over an evaluation period of T time steps as

$$F = \frac{1}{NTR} \sum_{t=0}^{T-1} \sum_{n=0}^{N-1} \sum_{r=0}^{R-1} 1 - |p_r^n(t) - s_r^n(t)|, \quad (1)$$

where N is the swarm size, R is the number of sensors per robot, $p_r^n(t)$ is the prediction for sensor r of robot n at time step t , and $s_r^n(t)$ is the value of sensor r of robot n at time step t .

1.2. Related Work

There are several conceptually similar approaches to minimal surprise ranging from machine learning to (swarm) robotics applications which make use of pairs of neural networks.

Ha and Schmidhuber [23, 24] train controllers using features extracted from a world model. This world model is implemented by a large recurrent neural network and trained by unsupervised learning independently from the controller. It predicts the future by determining a probability distribution of the next state based on information about its current state and current action. The controller is implemented as a perceptron and optimized by maximizing a task-specific reward using evolution strategies, for example, the agent is rewarded for visiting a maximum of tiles of the track in a minimum of time in the presented car racing scenario. The controller can even be trained entirely within hypothetical scenarios or ‘dreams’ generated by the world model. In that case, a world state is sampled from the probability distribution generated by the world model and is used as input for the next observation of the controller. In contrast to minimize surprise, Ha and Schmidhuber applied their approach to single agents in OpenAI Gym scenarios. As Ha and Schmidhuber train world models and controllers separately, different controllers can be trained using the same world model and independently from the actual environment. This is only possible as long as

single agent scenarios are considered. In collective systems, the world model depends not only on the (dynamic) environment but also on the existence and behavior of surrounding agents. The prediction network necessarily depends on the action network and they need to be evolved in pairs using minimize surprise. Furthermore, the world model used in Ha and Schmidhuber’s approach is represented by a large neural network and its training computational expensive.

Nolfi et al. [25, 26] combine learning during the lifetime of an individual with evolution across generations. The changes of the genome by learning at runtime are not inherited during evolution (cf. Lamarckian inheritance). They showed that learning has a beneficial effect on evolution by using different tasks for learning and evolution. In a sample setting, a single simulated agent has the evolutionary task to find food in a 2D grid world while its learning task is to predict the sensor values of the next time step, that is the next position of food. The reward given during learning in this setting is similar to the reward given in minimal surprise during evolution. Our learning process is completely driven by an intrinsic driver while Nolfi et al. rely on task-specific rewards.

Generative Adversarial Nets (GANs) were first proposed by Goodfellow et al. [27]. A generative model captures a data distribution while a discriminator estimates whether a sample is genuine or generated by the model. The generator is rewarded for tricking the discriminator to misclassify samples. This generates an adversarial process to estimate generative models. Goodfellow et al. represent both generator and discriminator as multilayer perceptrons and train them with backpropagation. Radford et al. [28], for example, used deep convolutional generative adversarial networks to learn general image representations in an unsupervised way.

Turing learning is conceptually similar to GANs [29, 30]. This system identification method allows machines to infer behaviors of natural or artificial systems without requiring predefined metrics. Two populations are optimized concurrently using coevolutionary algorithms: one population consists of models of the behavior of the system under investigation while the other consists of classifiers. The classifiers are rewarded for discriminating data between model and real system while models aim for tricking the classifier to categorize their data as genuine. Turing learning was applied to swarm robotics [30].

Neither GANs, Turing learning, nor minimize surprise make use of explicit reward functions. In contrary to minimize surprise, GANs and Turing learning aim to mimic an existing system based on genuine data samples.

Der, Martius, and Herrmann [31, 32] present the concepts of homeostasis and homeokinesis. In homeostasis both forward model and controller are trained by minimizing the prediction error which leads to a stabilized system. In homeokinesis, the objective was to create self-exploratory robots by introducing the time-loop error. This error destabilizes the system when activity stagnates and thus, enables self-exploration. Both concepts were studied in simulations and on real robots. Most of these tested robots were equipped with and reacted to proprioceptive sensors. In contrast to minimize surprise, in homeostasis the forward model and controller train each other by minimizing the prediction error which leads to a stabilized system.

Our minimal surprise approach aims for the evolution of collective robotics behaviors. We do not rely on task-specific rewards [24, 25] or data from a system to be imitated [29, 27]. In contrast to all of the above approaches, we do not train both networks explicitly. In minimize surprise, only the prediction network is rewarded directly while the action network is subject to genetic drift. In the standard version of our approach, we do not directly influence emerging behaviors and allow the evolutionary process to come up with own, creative solutions almost only in the form of a by-product of the evolutionary dynamics.

2. Methods

2.1. Experimental Setup for Self-Assembly

In previous works [19, 18], we found four basic swarm behaviors of rather low complexity using minimal surprise. We aim for the evolution of self-assembly behaviors to investigate more complex collective behaviors. To govern the difficulty of our initial study, we restrict us to a 2D torus grid world which simplifies sensing and the equidistant positioning of robots.

We conduct experiments with varying swarm densities (i.e., $\frac{N}{L \times L}$) by keeping a fixed swarm size $N = 100$ while changing the side lengths $L = \{15, 20\}$ of the square representing our torus grid environment following our previous approach [19]. In all evolutionary runs, we use a swarm size of $N = 100$, a population size of 50, proportionate selection, elitism of one, and a mutation rate of 0.1 for both networks. We run evolution for 100 generations and evaluate each genome ten times for 500 time steps with different initial robot positions. The fitness of a genome is the minimum fitness value (Eq. 1) of those ten evaluations.

We simulate a swarm of robots with discrete headings: North, East, South, and West. Using it’s action network, a robot selects either to move one grid cell forward or to rotate by $\pm 90^\circ$ in each time step. A robot can only move forward if the grid cell in front is empty as each grid cell can be occupied by only one robot at a time. Otherwise, an intended move forward is ignored and the robot stays on its current grid cell.

To evaluate the resulting behaviors, we measure the fitness of the genomes and the temperature T of the system during runtime. We define the temperature as the agents’ motion, that is, the covered distance of the robots per time step averaged over all robots. So the forward motion of robots is considered, while their rotations are ignored. This measurement roughly follows the concepts of thermodynamics where temperature is proportional to the average kinetic energy of the molecule’s center-of-mass motion [33]. The temperature cools down when there are more robots that stay on their grid cells, that is, they turn or are blocked in their forward movement. A hot system is in a disordered state with many moving robots and a cool system relates to a more ordered system which has assembled into a structure (cf. Ising model [34]).

We measure the robot movement M , that is the average covered distances and thus, the average temperature, of the robots over a time period of $\tau = \frac{L \times L}{2}$ time steps (cf. [35]). In addition, we determine the intended robot movement I ,

that is, the average distance over time period τ that all robots would have covered according to their selected action values if there were no obstacles.

The temperature T of the system at time step t is measured by summing up the robots' movements at that time step. We define T as

$$T(t) = M_x(t) + M_y(t), \quad (2)$$

where $M_x(t)$ and $M_y(t)$ are the movements in x - and y -direction of the grid in time step t .

We define $M_x(t)$ as

$$M_x(t) = \frac{1}{N} \sum_{n=0}^{N-1} |x_n(t) - x_n(t+1)|, \quad (3)$$

and M_y accordingly. This is the sum over the robots' movements, normalized by the number of robots N .

The robot movement M is the normalized sum of the system's temperature over the time period τ . We define the robot movement M as

$$M = \frac{1}{\tau} \sum_{t=T-\tau}^{T-1} T(t). \quad (4)$$

The simulation steps when robots chose the action value corresponding to moving one grid cell forward are counted and normalized as the intended robot movement

$$I = \frac{1}{N\tau} \sum_{n=0}^{N-1} \sum_{t=T-\tau}^{T-1} a_n(t), \quad (5)$$

where $a_n(t)$ is the action value of robot n at time step t , which is 1 for moving one grid cell forward and 0 for rotation. The robots are prevented to move straight when a targeted grid cell is occupied and thus, M and I can deviate.

2.2. Classification of Emergent Structures

We classify emerging structures based on the following metrics for eight different patterns: lines, pairs, aggregation, clustering, loose grouping, random dispersion, squares, and triangular lattices. In all following experiments, we categorize resulting structures based on the highest resemblance to one of these patterns.

Lines and pairs are structurally similar but differentiate in length. Lines have a minimum length of three robots while pairs consist of exactly two robots. The following rules apply to both structures:

1. The headings of all robots have to be parallel.
2. The structure has to be terminated by robots pointing inwards the structure at both ends.

3. The maximum number of allowed neighbors on each side next to the structure is half of the structure's length. Neighbors are not allowed to be positioned on two adjacent grid cells parallel to the structure.

Rule number two does not apply if a line spans the whole grid length, that is, it is a ring around the whole torus. The first two rules ensure that the formed structure is steady as robots stay in the structure when attempting to move straight.

We define three grouping behaviors: aggregation, clustering and loose grouping. A cluster is formed by robots which are connected by common neighbors in their Moore neighborhoods. A robot requires at least six neighbors in its Moore neighborhood to be a member of a cluster. Only one neighbor in the von Neumann neighborhood is allowed to be missing as only such can block the movement of another robot and trigger the formation of a steady structure. All neighbors of a robot in a cluster are considered as parts of that cluster and hence some robots at the border of a cluster might have less than six neighbors. This can lead to the fact that these robots are part of two clusters and connect them. Consequently, separate clusters are at least one grid cell apart. We define clustering as the formation of several separate clusters and aggregation as the formation of one single cluster. Completely interconnected clusters are considered as loosely grouped meaning that all clusters are either directly connected or connected via other clusters.

In addition, we define three dispersion behaviors: random dispersion, triangular lattices, and squares. The heading of the robots is not relevant for dispersion patterns as the robots have to constantly turn to stay on their grid cell. Each robot having maximally one neighbor in its Moore neighborhood is classified as randomly dispersed.

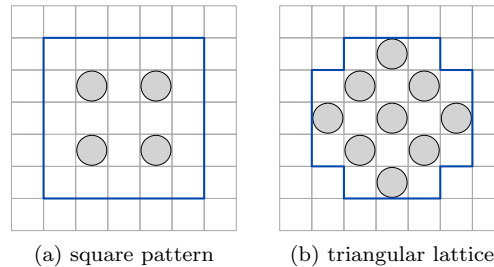


Figure 2: Square and triangular lattice pattern. Robots are represented by *gray circles*. *White cells* inside the areas marked by the *blue rectangles* have to be empty.

The square pattern is illustrated in Fig. 2a. The corners of the inner 3×3 grid are occupied by robots while all other grid cells in the surrounding 5×5 grid have to be empty. The triangular lattice pattern ensures that the robot in the center sees a rotation-symmetric pattern formed by its neighbors as shown in Fig. 2b. All robots within these patterns are classified to be part of the respective structure.

All defined metrics are based on the results of the experiments presented in the next sections. We automatically determine the resemblance to the individual patterns using Python scripts.

2.3. Sensor Model

We compare three different sensor models with discrete sensors in preliminary investigations to select a sensor model for all following experiments. Sensor model A covers a robot’s Moore neighborhood (see Fig. 3a), sensor model B the six grid cells in front of the robot (see Fig. 3b), and sensor model C 14 surrounding grid cells (see Fig. 3c). We evaluate each sensor model in 20 independent evolutionary runs and classify the resulting structures based on the metrics presented in Sec. 2.2.

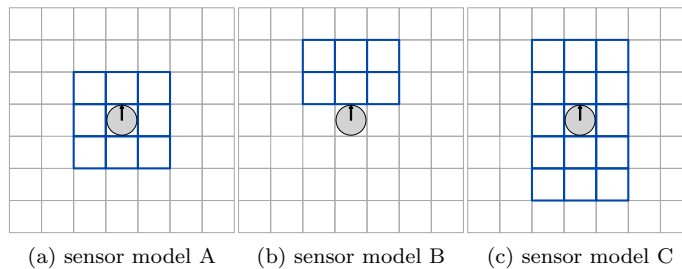


Figure 3: Sensor models evaluated in preliminary investigations. *Gray circles* represent robots, *black arrows* indicate their headings.

	lines	aggre- gation	clustering	loose grouping	triang. lattice	pairs
sensor model A	10	5	30	25	20	10
sensor model B	30	15	35	15	0	5
sensor model C	15	10	55	15	5	0

Table 1: Percentage of resulting structures on a 15×15 grid per sensor model.

	pairs	lines	clustering	random dispersion	squares
sensor model A	5	0	5	75	15
sensor model B	35	65	0	0	0
sensor model C	27.5	22.5	10	40	0

Table 2: Percentage of resulting structures on a 20×20 grid per sensor model.

On the 15×15 grid, all three sensor models lead to the emergence of a variety of behaviors, cf. Table 1. In comparison to sensor model A, sensor model B did not lead to the emergence of triangular lattices while no pairs emerged using

sensor model C. On the 20×20 grid the difference between the sensor models becomes more significant, cf. Table 2. Sensor model B resulted solely in the emergence of lines and pairs. Both sensor models A and C led to the emergence of four different structures. No line structures, but a majority of dispersion behaviors emerged using sensor model A. In contrast, using sensor model C led to the formation of lines and pairs in many cases and in less cases to dispersion behaviors. We use sensor model C in all following experiments as it enables us to evolve varieties of structures independent from swarm density. We reference the individual sensors of sensor model C as indicated in Fig. 4.

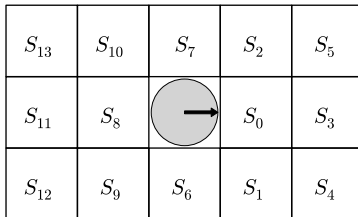


Figure 4: Labels for the individual sensors of sensor model C. The *gray circle* represents the robot and the *black arrow* its heading. Reprinted by permission from Springer Nature Customer Service Centre GmbH: [21], ©Springer Nature Switzerland AG 2019.

Due to the chosen sensor model, both networks have 15 input neurons each. Furthermore, the action network has eight hidden neurons and two output neurons which determine action value and turning direction. The prediction network has 14 hidden neurons and 14 output neurons which give the discrete predictions for the 14 sensors.

We evaluate all following experiments in 50 independent evolutionary runs. Table 3 summarizes the parameters of the evolutionary runs.

parameter	value
grid side length L	{15, 20}
# of sensors R	14
swarm size N	100
population size	50
number of generations	100
evaluation length in time steps T	500
# of sim. runs per fitness evaluation	10
elitism	1
mutation rate	0.1

Table 3: Parameter settings [21].

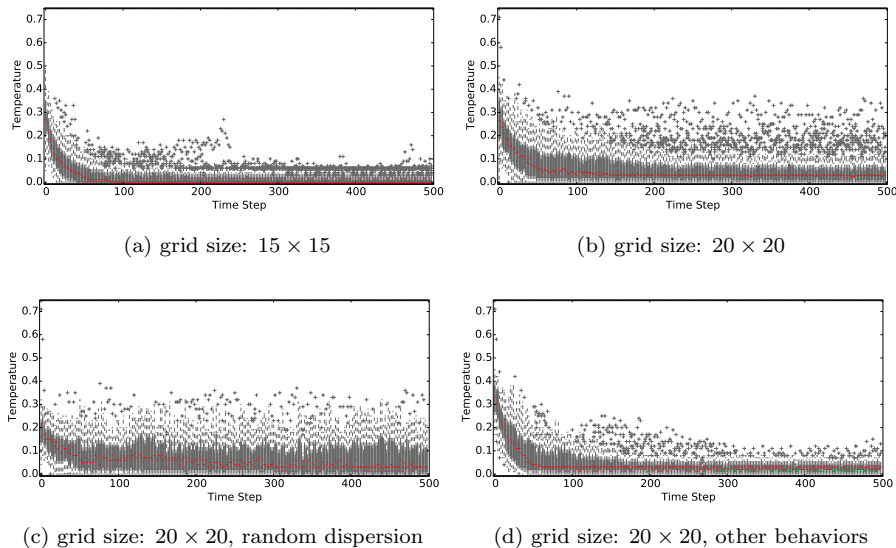


Figure 5: Temperature of 50 independent runs. Medians are indicated by *red bars*. Only data of even time steps is plotted.

3. Results

3.1. Impact of Varying Swarm Densities

We investigate the effects of different swarm densities on the emergence of structures in two scenarios. In the first setting, we use a 15×15 grid resulting in a swarm density of approx. 0.44 while we have a swarm density of 0.25 in the second scenario using a 20×20 grid. A video illustrating the resulting self-assembly behaviors is available online¹.

The measured temperature (Eq. 2) shown in Fig. 5 illustrates how the systems cool down over time. Already after around 100 time steps almost all robots are staying stopped and thus, the robots quickly assemble into a structure. We measure a median temperature value of 0.03 on the 20×20 grid and of zero on the 15×15 grid in the last time step meaning that 3% and 0%, respectively, of the robots moved one grid cell forward. The outliers in Fig. 5b are mostly caused by random dispersion behaviors. This is illustrated in Figs. 5c and 5d which show the measured temperature separately for random dispersion behaviors and all other behaviors. A reason might be that robots attempt to spread as widely apart as possible, but the swarm density does not allow to have no neighbors within sensor view. On the 15×15 grid, no random dispersion behaviors emerge (cf. Table 4) and thus, there are less outliers in the temperature curve.

¹<https://youtu.be/pCcg6zdR9A>

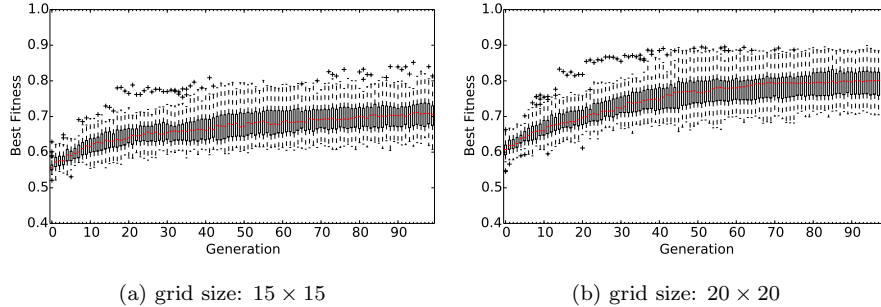


Figure 6: Best fitness of 50 independent runs. Medians are indicated by the *red bars*. Reprinted by permission from Springer Nature Customer Service Centre GmbH: [21], ©Springer Nature Switzerland AG 2019.

Figure 6 shows the increase of the best fitness over generations for both swarm densities and is representative for the fitness curves observed in all experiments. For the experiments on the 15×15 grid, the median best fitness of the last generation is 0.71 and 0.80 for the 20×20 grid meaning that the prediction network assesses about 71% and 80%, respectively, of the sensor values correctly. Thus, the prediction task gets easier for sparse swarm densities.

	cluster	aggregation	loose grouping	lines	pairs	triang. lattice
% of structures	44	12	16	20	2	6
% of robots in structure	92.8 (93.0)	96.5 (96.5)	95.5 (96.5)	49.7 (49.0)	30.0 (30.0)	64.7 (64.0)
fitness F	0.701 (0.704)	0.695 (0.69)	0.7 (0.708)	0.708 (0.698)	0.707 (0.707)	0.751 (0.764)
movement M	0.008 (0.0)	0.01 (0.0)	0.003 (0.0)	0.019 (0.012)	0.02 (0.02)	0.03 (0.029)
intended movement I	0.911 (0.927)	0.865 (0.947)	0.901 (0.926)	0.849 (0.838)	0.816 (0.816)	0.05 (0.063)

Table 4: Mean best fitness over 500 time steps, percentage of robots within the structure in the last time step, robot movement, and intended robot movement in the last 113 time steps by emerging structures on a 15×15 grid, median values in brackets.

We classify various emergent structures in our experiments, see Figs. 7 and 8, based on the metrics defined in Sec. 2.2. For higher swarm densities (smaller grid), mostly grouping behaviors evolve, see Table 4 and Fig. 7, while for low densities (larger grid) many randomly dispersed structures emerge, see Table 5 and Fig. 8. On the 15×15 grid, nearly all robots assemble into the grouping structures while the number is lower in lines, pairs and triangular lattices. On the larger grid, the median percentage of robots assembling into line structures is higher than on the smaller grid. On average, more than 60% of robots assemble

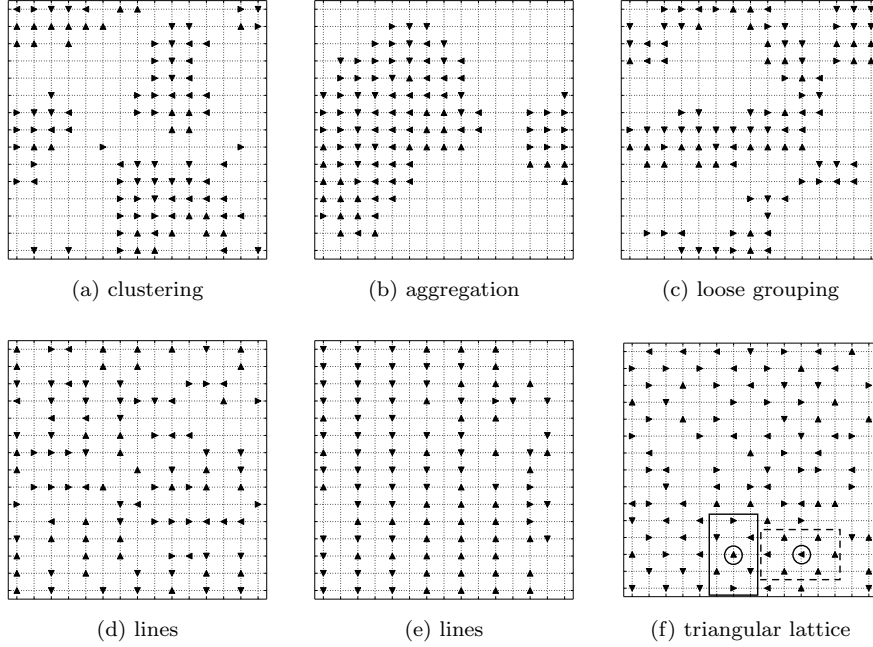


Figure 7: Resulting structures on a 15×15 grid, the *rectangles* in (f) give the sensor view of the encircled robot as example. The *triangles* give the robots' headings. Reprinted by permission from Springer Nature Customer Service Centre GmbH: [21], ©Springer Nature Switzerland AG 2019.

into the resulting structures on the 20×20 grid.

On the 15×15 grid, emerging line structures span over the whole torus in 20% of the runs in which lines form while this is not observed on the 20×20 grid. Triangular lattices solely emerge in the smaller grid, as the swarm density on the larger grid is too small to allow the formation of a repetitive triangular pattern over most of the grid. Nevertheless, a tendency towards triangular lattices is visually observable in 6% of the runs, as illustrated in Fig. 8c. Similarly, the square pattern can be visually observed in 6% of the runs as shown in Fig. 8b with a median of 19% of robots assembling into the structure. All of those runs are classified as random dispersion. In summary, the swarm density has a strong influence on the emerging structures.

A comparison of mean robot movement (Eq. 4), mean intended robot movement (Eq. 5), and mean fitness (Eq. 1) of the resulting structures within the best evolved individuals enables us to identify differences in their behavioral characteristics, see Tables 4 and 5. We observe a similar mean fitness for all emerging structures, whereby it is slightly higher in the experiments on the larger grid. In clustering, aggregation, loose grouping, line structures and pairs the intended movement I is high while the robot movement M is low. Robots keep their positions and headings if the grid cell in front is occupied and they intend to

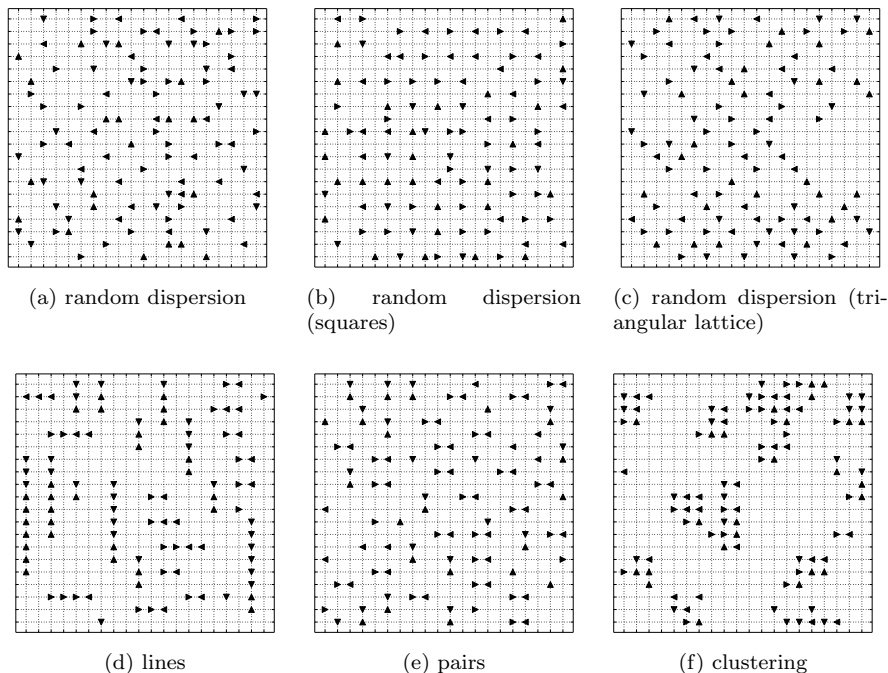


Figure 8: Resulting structures on a 20×20 grid. The *triangles* give the robots' headings. Reprinted by permission from Springer Nature Customer Service Centre GmbH: [21], ©Springer Nature Switzerland AG 2019.

move straight, which happens frequently in those structures. Thus, the robots' sensor values are mostly constant and can be easily predicted. Robots favor rotations in triangular lattices and random dispersion, that is, I and M are low. In triangular lattices, each robot has the same sensory perception in every orientation as illustrated in Fig. 7f. Thus, robots can keep their sensor values constant by turning meaning that these behaviors are evolutionary stable, too. Overall, the robots' movement is low for all structures in the last τ time steps. This is supported by the temperature curve, see Fig. 5, which shows that almost all robots stay stopped after 100 time steps in both swarm densities.

We aim to find the relationship between the world model of the robot and the emergent structures. Therefore, we assess the average sensor predictions during the evolutionary run of the best individuals which correspond to the robot's anticipated environment. In grouping behaviors like aggregation (see Fig. 9a), clustering and loose grouping, robots predict that the majority of their adjacent grid cells are occupied. In contrast, none of the adjacent grid cells are predicted to be occupied when forming random dispersion, see Fig. 9b. Robots predict that the grid cells in front and behind of them are occupied for line structures as shown in Fig. 9c. Forming pairs, a neighbor is only expected to be sensed on the grid cell directly in front of a robot. The sensor predictions in

	lines	pairs	random dispersion	clustering
% of structures	25	27	42	6
% of robots in structure	66.3 (65.0)	61.57 (62.0)	61.6 (65.0)	65.3 (67.0)
fitness F	0.833 (0.838)	0.821 (0.812)	0.779 (0.79)	0.734 (0.734)
movement M	0.017 (0.016)	0.043 (0.049)	0.074 (0.065)	0.021 (0.027)
intended movement I	0.966 (0.978)	0.886 (0.905)	0.128 (0.125)	0.98 (0.979)

Table 5: Mean best fitness over 500 time steps, percentage of robots within the structure in the last time step, robot movement, and intended robot movement in the last 200 time steps by emerging structures on a 20×20 grid, median values in brackets.

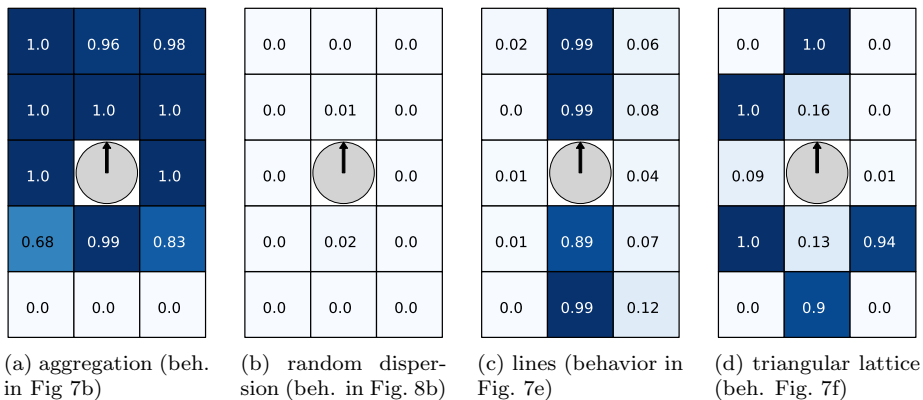


Figure 9: Average sensor predictions of all 100 robots over 500 time steps for resulting behaviors shown in Figs. 7 and 8. Robots are represented by *gray circles*, *black arrows* indicate their headings. Reprinted by permission from Springer Nature Customer Service Centre GmbH: [21], ©Springer Nature Switzerland AG 2019.

triangular lattices follow this intuitive scheme, too, and match almost completely the visually observed robot structure as shown in Fig. 9d. Thus, we find that the robots’ world models (i.e. their average sensor predictions) and the observed structures coincide closely.

3.2. Engineering Self-Organized Self-Assembly

A strength of our minimal-surprise approach is the emergence of non-trivial swarm behaviors, despite selective pressure to minimize the prediction error. Another strength is that the evolutionary process can be easily manipulated to push towards the emergence of wanted behaviors. We predefine several or even all of the robots’ sensor value predictions by fixing some or all outputs p_0, \dots, p_{R-1} of the prediction network to desired values. High fitness values are than achieved by good predictions of the unfixed outputs p_r (if any) and by appropriate behaviors. We measure the success by investigating the impact on the resulting structures. In our initial experiments, we keep the swarm size of $N = 100$ and the grid side lengths of $L = \{15, 20\}$. Without loss of generality, we aim for the emergence of lines. A video is available online² and shows the self-assembly behaviors.

We partially predefine prediction values in the first step. We set the predictions of the sensors in front and behind the robot to 1 (i.e., $S_0 = S_3 = S_8 = S_{11} = 1$, cf. Fig. 4) while the other ten remaining sensors still need to be predicted by the prediction network. Thus, the prediction network has 15 input neurons, 12 hidden neurons, and ten output neurons. To obtain a converging fitness curve, the mutation rate was adjusted to 0.3 for the runs on the 20×20 grid. For the 15×15 grid, the median best fitness of the last generation is 0.72 and for the 20×20 grid 0.78.

We notice a decrease in the variety of resulting structures by partially predefining sensor predictions. The best evolved individuals lead to clustering, aggregation and loose grouping in 64% and to the formation of lines in 36% of the runs on the 15×15 grid. Thus, we observe an increase of 16% in the formation of line structures and a decrease of 8% in grouping behaviors compared to running the approach without predefining any sensor predictions. Pairs and triangular lattice behaviors do not emerge anymore. On the 20×20 grid, robots cluster in 8%, form pairs in 2% and form lines in 90% of the runs. Consequently, we notice an increase of 2% in clustering and of 65% in the formation of lines. Pairs form only in one run and no random dispersion as well as no triangular lattices emerge as a consequence of predefining the sensors in front and behind the robot to 1. The average sensor value predictions of these structures deviate at least in two of the four predefined values, cf. Fig 9. Grouping behaviors can easily emerge in this scenario as a robot requires more than four neighbors for these structures and thus, just predicts more cells to be occupied. We observe that in the emergent grouping behaviors the average sensor predictions of all robots are above 0.5 for at least three of the ten sensors which are still predicted

²<https://youtu.be/XYZgqPYt-kY>

by the prediction network on the 15×15 grid and for at least four sensors on the 20×20 grid, respectively. An average sensor prediction above 0.5 states that a grid cell is predicted to be occupied by all robots in at least half of the time steps. Similarly, for line structures on the 15×15 grid maximally two of the sensors and, respectively, three sensors on the 20×20 are on average predicted above 0.5 as the predefined predictions already match the structure.

Overall, the emergence of lines increases and thus, we successfully engineered an influence on the emerging structures. However, we cannot avoid a dependence on the environment (robot density). As before, we observe lines spanning over the whole torus in 67% of the runs resulting into line structures on the smaller grid while none are observed on the larger grid.

Next, we predefine all sensor predictions of the robots while still aiming for the emergence of line structures. In consequence, the prediction network is not evolved anymore. We rely exclusively on the action network being subject to genetic drift by keeping the fitness as defined in Eq. 1. As before, we predefine the sensor predictions in front and behind the robot to 1 while we set all other sensor value predictions to 0 now. The median best fitness of the last generation is 0.85 on the 15×15 grid and 0.88 on the 20×20 grid.

In the runs, we measure additionally the quantity of emergent horizontal, vertical and maze-like line structures. Resulting line structures are categorized as mostly horizontal or mostly vertical when more than two thirds of the resulting lines are formed horizontally or vertically, respectively. Otherwise the resulting line structure is categorized as maze-like.

We achieve line structures in all runs for both grid sizes (see Fig. 10) with a median of 66.5% of robots within the structure on the 15×15 grid and a median of 89% on the 20×20 grid. The line structures span over the whole torus on the 15×15 grid in 68% of the runs (Fig. 10a), while this is not observed on the 20×20 grid. On the 15×15 grid, the best robots self-assemble in mostly horizontal lines and into mostly vertical lines in 28% of the cases each and in 44% in maze-like line structures. The best robots self-assemble both into mostly horizontal lines and into mostly vertical lines in 22% of the runs on the 20×20 grid and form maze-like line structures in 56% of the runs. Thus, the ANN pairs lead to the formation of a variety of line structures.

We investigate the effect of the environment on emerging structures as the geometry of our torus environment (i.e. ratio of one diameter to the other) can have an influence. Thus, we switch from square to rectangular grids. We still aim for biasing the emergence towards lines and predefine all sensor predictions as before. We use $N = 100$ robots on a 25×8 grid which leads to a swarm density of 0.5. The robots can either self-assemble into horizontal lines (along the longer diameter of the torus) or vertical lines (along the shorter diameter) to reach maximum fitness values in this scenario. The median best fitness of the last generation is 0.82 in 50 independent evolutionary runs.

The best robots self-assemble into mostly horizontal lines in 16% of the runs (Fig. 11a), in 32% of the runs into mostly vertical lines (Fig. 11b), and in the remaining 52% into maze-like line structures (Fig. 11c).

Compared to the 15×15 grid, which has a similar swarm density, we observe

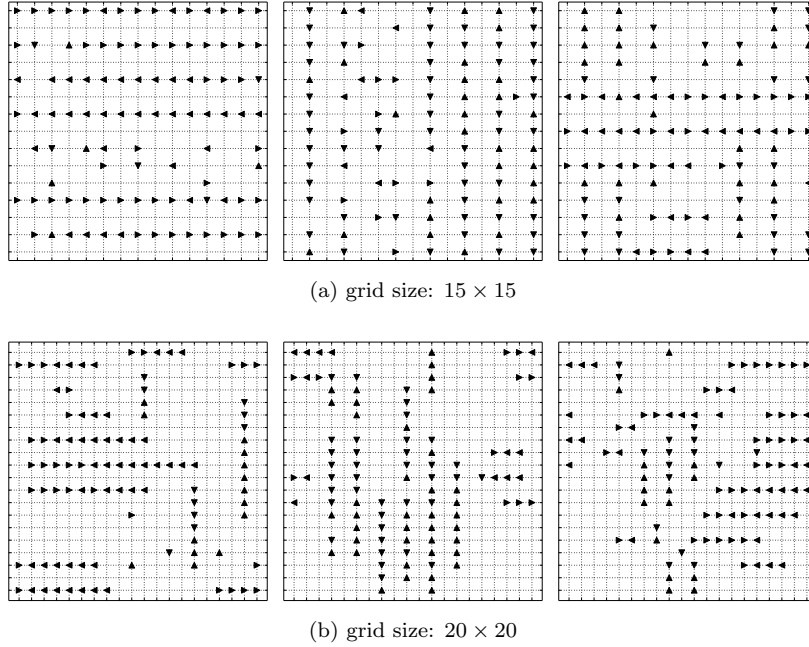


Figure 10: Resulting structures with predefined predictions. The *triangles* give the robots' headings. Mostly horizontal lines, mostly vertical lines, and maze-like line structures (left to right).

an increase in the formation of vertical lines and a decrease in the formation of horizontal lines on the 25×8 grid. The overall formation of horizontal and vertical lines decreases slightly from 56% to 48%. But the number of runs in which lines spanning the whole grid length formed increased from 68% on the 15×15 grid to 98% on the 25×8 grid. Maybe because one grid length is much smaller, grid-spanning lines can be formed more easily. Nevertheless, both vertically and horizontally grid-spanning lines were formed.

We use an 11×18 grid resulting in a swarm density of approx. 0.51 to increase the bias towards horizontal lines. Theoretically, the best possible fitness can be reached if the robots self-assemble into nine lines with 11 robots each and thus, one robot would be left without a proper spot. The median best fitness of the last generation is 0.81.

In 42% of the cases, the best evolved individuals result in the emergence of mostly horizontal lines (Fig. 12a), of vertical lines in 4% (Fig. 12b), and of maze-like line structures in 54% (Fig. 12c). We have successfully biased evolution towards horizontal lines as they emerge frequently here. Lines spanning the whole grid length formed in 88% of the runs including all runs where mostly horizontal or vertical lines formed.

Last, we re-evaluate the best individuals of all presented evolutionary runs with completely predefined sensor predictions using new starting positions in

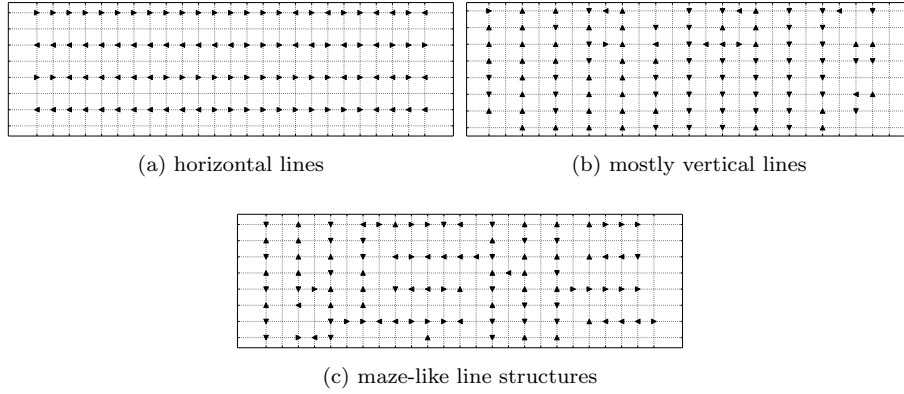


Figure 11: Resulting structures on a 25×8 grid with predefined predictions. The *triangles* give the robots' headings. Figs. 11a and 11b reprinted by permission from Springer Nature Customer Service Centre GmbH: [21], ©Springer Nature Switzerland AG 2019.

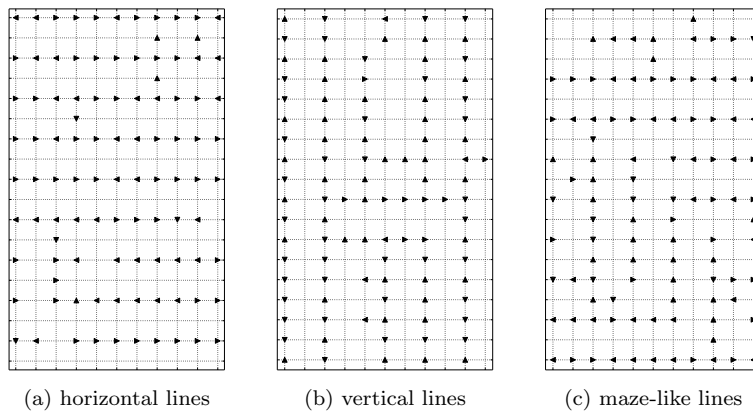


Figure 12: Resulting structures on an 11×18 grid with predefined predictions. The *triangles* give the robots' headings. Figs. 12a and 12b reprinted by permission from Springer Nature Customer Service Centre GmbH: [21], ©Springer Nature Switzerland AG 2019.

20 independent runs. This enables us to analyze the influence of the robots’ starting positions on the formation of line structures. An ANN pair is considered to form vertical, horizontal or maze-like lines, respectively, if more than half of these evaluations lead to the formation of such line structures. Otherwise, the ANN pair is classified as forming diverse line structures.

grid size		vertical	horizontal	maze-like	diverse
15×15	initial run	28	28	44	0
	new initial position	2	14	14	70
20×20	initial run	22	22	56	0
	new initial position	2	2	36	60
25×8	initial run	32	16	52	0
	new initial position	38	6	30	26
11×18	initial run	4	42	52	0
	new initial position	0	52	36	12

Table 6: Percentage of mostly horizontal, mostly vertical and maze-like line structures when predefining all sensor predictions. Values of all 50 initial runs and the re-evaluation of the resulting ANN pairs with new starting positions are given.

Both on the 15×15 grid and on the 20×20 grid, we observe a decrease in the quantity of ANN pairs which lead to the formation of lines in a certain structure, i.e. vertical, horizontal or maze-like. 70% of the evolved ANN pairs on the 15×15 grid and 60% on the 20×20 grid lead to the formation of diverse line structures, cf. Table 6. In contrary, on the 25×8 grid the amount of ANN pairs forming vertical and horizontal lines stays similar while the quantity of genomes leading to maze-like line structures drops by 22%. On the 11×18 grid, the percentage of horizontal lines increases by 10% in the evaluations with new starting positions while only 12% of the ANN pairs lead to the formation of diverse line structures. Thus, while the initial positions of the robots influences the formation of the final structure, we observe a stronger influence by the shape of the environment³.

Overall, (partially) predefining sensor predictions or changing the environment enables us to bias the evolutionary process, despite the intrinsic driver of minimizing surprise. Thus, we can trigger the emergence of desired self-assembly behaviors by engineering self-organization.

3.3. Resilience of Self-assembly Behaviors

In a last series of experiments, we investigate the resilience of the various emergent self-assembly behaviors. We damage the structure by removing or repositioning robots from an area for two of the evolved self-assembly behaviors:

³Please note that this re-evaluation of the genomes with new starting positions led to the classification of 0.7% (7 out of 1000 runs) as random dispersion on the 15×15 grid and to pairs in 0.1% (1 out of 1000 runs) on both the 25×8 grid and the 11×18 grid.

the behaviors forming the line structures shown in Fig. 7e and the triangular lattices shown in Fig. 7f. A video is available online⁴.

We evaluate both behaviors using three scenarios. First, we rerun the controller and world model pair using new random starting positions showing structures form independent from initial robot positions. In a second step, we damage one part of the structure by removing several robots from the assembled structure. Last, we randomly replace all robots from a certain area of the structure.

In each scenario, the controller and world model pair is evaluated for another 500 time steps after the damage. We run 20 independent runs for each scenario in the first and the last scenario, while we do one run in the second case as each repetition leads to the same result due to our completely deterministic simulation environment.

We measure the fitness (cf. Eq. 1) and the percentage of robots which are assembled into the pattern at the start and the end of running the simulation for another 500 time steps realizing the above described scenarios (cf. Sec. 2.2). Additionally, we measure the similarity of the resulting structure to the initial structure. For line structures, this is the number of robots with equal positions and headings normalized by the swarm size $N = 100$. Only the position is taken into account for triangular lattices as in this structure robots constantly turn to stay on their grid cell, cf. Sec. 3.1.

We first analyze the resilience of the line formation behavior shown in Fig. 7e. A few robots are not part of the structure as they still move. The formed structure is not steady, however, a total of 82% of the robots assemble into lines in this run.

	fitness	% of robots in structure (start)	% of robots in structure (end)	similarity
initial run	0.814	0	0.82	1.0
new starting position	0.855 (0.850)	0.013 (0.0)	0.833 (0.86)	0.099 (0.02)
remove area A	0.958	0.693	0.795	0.76
remove area B	0.94	0.494	0.904	0.57
remove area C	0.939	0.652	0.891	0.72
reposition area A	0.915 (0.917)	0.494 (0.54)	0.835 (0.865)	0.588 (0.6)
reposition area B	0.905 (0.913)	0.322 (0.365)	0.839 (0.86)	0.392 (0.415)
reposition area C	0.903 (0.932)	0.562 (0.6)	0.862 (0.87)	0.587 (0.585)

Table 7: Resilience of line structures: mean fitness in 500 time steps, percentage of robots in the structure at the start and the end of the run and similarity of the assembled structure to the initial structure. Median values in brackets.

⁴<https://youtu.be/KWJIgPZd060>

First, we rerun the robots with the respective ANN pair using new random starting positions. We measure an increase in fitness and almost all robots form line structures, see Table 7. The fitness value of the reruns is higher as the fitness of the initial run is the minimum of ten repetitions, cf. Sec. 1.1. The median fitness is higher than in the initial run for the other scenarios as well. In these runs, the robots have the advantage to be mostly positioned in the structure at the beginning of the run compared to random starting positions. Thus, the predictions of the robots’ world model, cf. 9c, matches more closely from the start of the run and a higher fitness can be reached.

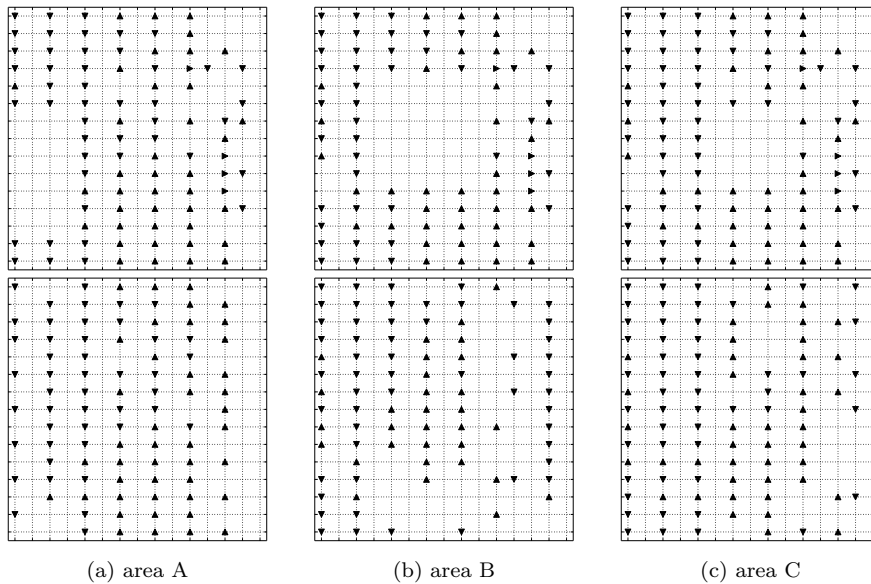


Figure 13: Test for resilience, damage by removing robots from different areas in line structures; starting positions top, final positions bottom.

Next, we remove robots from three different areas of the structure, see Fig. 13. We remove 12 (see Fig. 13a), 17 (see Fig. 13b) and eight (see Fig. 13c) robots, respectively. In all three cases, the percentage of robots within the structure drops due to the removal of robots by at least 13%. We run the controller for another 500 time steps and observe that the percentage of robots within the structure increases again and reaches even higher levels than in the initial structure in two out of three cases. Furthermore, line structures form in the removed area again, see Fig. 13, and we find a high resemblance to the original structure in two out of three runs.

Now we reposition the robots instead of removing them from the three areas. The swarm density stays constant and robots have to coordinate with more other robots than in the tests above. The percentage of robots in the structure reduces by at least 25%, cf. Table 7. In all three scenarios, the percentage of

	fitness	% of robots in structure (start)	% of robots in structure (end)	similarity
initial run	0.764	0	0.63	1.0
new starting position	0.78 (0.781)	0.0 (0.0)	0.77 (0.78)	0.468 (0.46)
remove area A	0.763	0.609	0.586	0.39
remove area B	0.761	0.671	0.659	0.52
remove area C	0.791	0.663	0.761	0.67
reposition area A	0.789 (0.788)	0.218 (0.225)	0.752 (0.805)	0.564 (0.62)
reposition area B	0.791 (0.791)	0.164 (0.18)	0.782 (0.8)	0.545 (0.605)
reposition area C	0.798 (0.798)	0.384 (0.395)	0.793 (0.805)	0.571 (0.61)

Table 8: Resilience of triangular lattices: mean fitness in 500 time steps, percentage of robots in the structure at the start and the end of the run and similarity of the assembled structure to the initial structure. Median values in brackets.

robots within the structure increases again and is at least 0.015 higher than in the initial structure in the last time step. However, the similarity to the initial structure does not reach a higher median value than 60%.

As a second example, we show the resilience of the behavior leading to the formation of triangular lattices as illustrated in Fig. 7f. As before, we observe an increase in the fitness and a high percentage of robots is part of the structure rerunning the controller with new initial starting positions, see Table 8.

We remove three different areas from the structure, cf. Fig. 14. Thus, 13 (see Fig. 14a), 15 (see Fig. 14b) and eight (see Fig. 14c) robots, respectively, are removed from the structure. This leads to an immediate increase of the percentage of robots within the structure for two out of three scenarios which indicates that robots which were not part of the structure got removed. In one case, this percentage increases after rerunning the controller while in the other two cases it even decreases. In these two cases, more robots got removed and thus, the swarm density might be too low for the formation of a repetitive pattern.

We reposition the robots from the three areas in the next step which leads to a major decrease of robots being part of the triangular lattice. In all three scenarios, we observe an increase of the number of robots within the structure by at least 12% compared to the initial structure and an intermediate similarity to the initial structure. Thus, the robots reassemble to form the same pattern as in the initial run, but do not position themselves on the same grid cells. In total, we observe that the evolved self-assembly behaviors are resilient as removing or repositioning robots leads to the reassembly of the pattern.

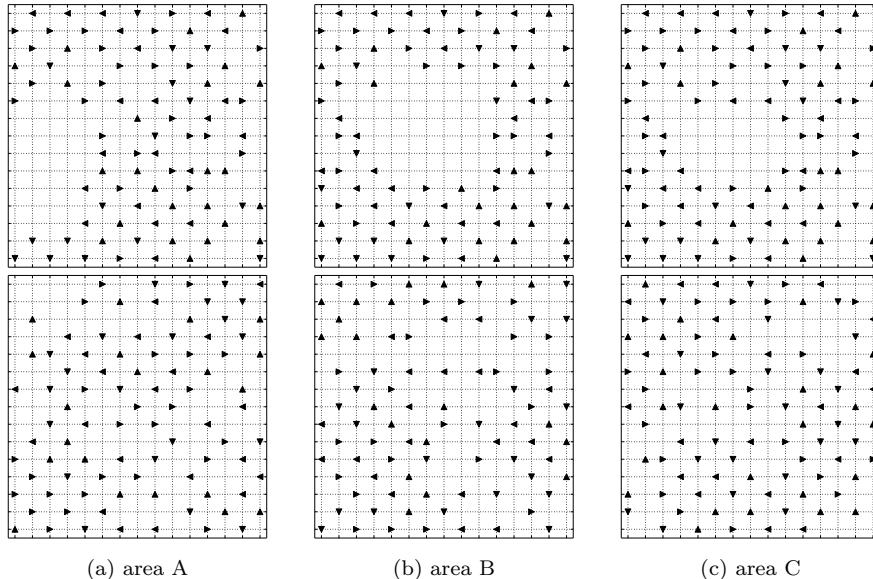


Figure 14: Test for resilience, damage by removing robots from different areas of triangular lattice structures; starting positions top, final positions bottom.

4. Discussion and Conclusion

In our study, we observe different self-assembly behaviors depending on the swarm density for the case of not predefining any predictions, that is, the approach is run with complete freedom. For high densities, we find mostly grouping behaviors (aggregation, clustering, etc.) and for intermediate densities a wide variety of behaviors (lines, dispersion, triangular lattices, etc.). Thus, too high and too low swarm densities generate rather trivial collective behaviors which is in line with our previous findings [19]. The predictions of the robots are complicated by densities in between, which may lead to the emergence of more complex behaviors to still achieve ordered and easy to predict patterns.

The (partially) engineered approach of predefining the prediction network’s outputs successfully biases towards desired self-organizing collective behaviors. We find different collective self-assembly behaviors based on the density and/or the shape of the environment (here, the relation of the short radius to the long radius of the torus), that is, an adaptation to the environment. Furthermore, we find that the evolved self-assembly behaviors are resilient and lead to the reassembly of the pattern when removing or replacing robots.

We are confident to switch our grid-based self-assembly simulation to continuous space in future work. Furthermore, we will analyze the resulting networks in more detail, investigate the influence of heterogeneous swarms on the emerging behaviors, and explore how self-assembly behaviors can be evolved that lead to the formation of more complex patterns while minimizing surprise.

In ongoing work, we conduct first experiments to prepare our approach for swarm robot experiments. Instead of the evolutionary approach, we make use of machine learning techniques (backpropagation). The prediction network of a robot can be trained with unsupervised learning using a robot's own predictions and sensor readings [24]. Additionally, we switch from an action ANN to a simple rule set. In initial experiments using a single Thymio II robot [36], we were able to train the prediction network and a wall following behavior emerged. In future work, we aim to learn more complex behaviors on a single robot as well as to extend it to a swarm scenario such that complex multi-robot behaviors can arise on top of a mere unsupervised learning process driven by minimizing surprise.

References

- [1] H. Hamann, *Swarm Robotics: A Formal Approach*, Springer, 2018. doi: 10.1007/978-3-319-74528-2.
- [2] M. Brambilla, E. Ferrante, M. Birattari, M. Dorigo, Swarm robotics: a review from the swarm engineering perspective, *Swarm Intelligence* 7 (1) (2013) 1–41. doi:10.1007/s11721-012-0075-2.
URL <http://dx.doi.org/10.1007/s11721-012-0075-2>
- [3] V. Trianni, *Evolutionary Swarm Robotics - Evolving Self-Organising Behaviours in Groups of Autonomous Robots*, Vol. 108 of *Studies in Computational Intelligence*, Springer, Berlin, Germany, 2008. doi:10.1007/978-3-540-77612-3.
- [4] L. Busoniu, R. Babuska, B. De Schutter, A comprehensive survey of multi-agent reinforcement learning, *IEEE Transactions on Systems, Man, And Cybernetics-Part C: Applications and Reviews* 38.
- [5] L. Panait, S. Luke, Cooperative multi-agent learning: The state of the art, *Autonomous Agents and Multi-Agent Systems* 11 (3) (2005) 387–434.
- [6] S. Doncieux, N. Bredeche, J.-B. Mouret, A. E. G. Eiben, Evolutionary robotics: What, why, and where to, *Frontiers in Robotics and AI* 2 (2015) 4. doi:10.3389/frobt.2015.00004.
URL <https://www.frontiersin.org/article/10.3389/frobt.2015.00004>
- [7] D. Silver, T. Hubert, J. Schrittwieser, I. Antonoglou, M. Lai, A. Guez, M. Lanctot, L. Sifre, D. Kumaran, T. Graepel, T. Lillicrap, K. Simonyan, D. Hassabis, A general reinforcement learning algorithm that masters chess, shogi, and go through self-play, *Science* 362 (6419) (2018) 1140–1144. arXiv:<http://science.sciencemag.org/content/362/6419/1140.full.pdf>, doi:10.1126/science.aar6404.
URL <http://science.sciencemag.org/content/362/6419/1140>

- [8] J. K. Gupta, M. Egorov, M. Kochenderfer, Cooperative multi-agent control using deep reinforcement learning, in: International Conference on Autonomous Agents and Multiagent Systems, Springer, 2017, pp. 66–83.
- [9] T. Taylor, M. Bedau, A. Channon, D. Ackley, W. Banzhaf, G. Beslon, E. Dolson, T. Froese, S. Hickinbotham, T. Ikegami, et al., Open-ended evolution: perspectives from the oee workshop in york, *Artificial life* 22 (3) (2016) 408–423.
- [10] K. Ruiz-Mirazo, J. Umerez, A. Moreno, Enabling conditions for ‘open-ended evolution’, *Biology & Philosophy* 23 (1) (2008) 67–85.
- [11] J. C. Bongard, Evolutionary robotics, *Communications of the ACM* 56 (8) (2013) 74–83. doi:10.1145/2493883.
- [12] J. Lehman, K. O. Stanley, Exploiting open-endedness to solve problems through the search for novelty, in: S. Bullock, J. Noble, R. Watson, M. A. Bedau (Eds.), *Artificial Life XI: Proceedings of the Eleventh International Conference on the Simulation and Synthesis of Living Systems*, MIT Press, 2008, pp. 329–336.
- [13] A. L. Nelson, G. J. Barlow, L. Doitsidis, Fitness functions in evolutionary robotics: A survey and analysis, *Robotics and Autonomous Systems* 57 (2009) 345–370.
- [14] S. Doncieux, J.-B. Mouret, Beyond black-box optimization: a review of selective pressures for evolutionary robotics, *Evolutionary Intelligence* 7 (2) (2014) 71–93.
- [15] M. Divband Soorati, H. Hamann, The effect of fitness function design on performance in evolutionary robotics: The influence of a priori knowledge, in: Genetic and evolutionary computation conference (GECCO 2015), ACM, 2015, pp. 153–160.
- [16] Á. E. Eiben, J. E. Smith, *Introduction to Evolutionary Computing*, Natural Computing Series, Springer, 2003.
- [17] K. Friston, The free-energy principle: a unified brain theory?, *Nature Reviews Neuroscience* 11 (2) (2010) 127–138. doi:10.1038/nrn2787.
- [18] R. Borkowski, H. Hamann, Evolving robot swarm behaviors by minimizing surprise: results of simulations in 2-d on a torus, in: *Evolving Collective Behaviors in Robotics Workshop, GECCO 2017*, ACM, 2017, pp. 1679–1680. doi:10.1145/3067695.3082548.
- [19] H. Hamann, Evolution of collective behaviors by minimizing surprise, in: H. Sayama, J. Rieffel, S. Risi, R. Doursat, H. Lipson (Eds.), *14th Int. Conf. on the Synthesis and Simulation of Living Systems (ALIFE 2014)*, MIT Press, 2014, pp. 344–351.

- [20] P. Zahadat, H. Hamann, T. Schmickl, Evolving diverse collective behaviors independent of swarm density, in: Workshop Evolving Collective Behaviors in Robotics (GECCO 2015), ACM, 2015, pp. 1245–1246, [extended abstract]. doi:10.1145/2739482.2768492.
- [21] T. K. Kaiser, H. Hamann, Self-assembly in patterns with minimal surprise: Engineered self-organization and adaptation to the environment, in: N. Correll, M. Schwager, M. Otte (Eds.), Distributed Autonomous Robotic Systems, Springer International Publishing, Cham, 2019, pp. 183–195.
- [22] J. H. Holland, Adaptation in Natural and Artificial Systems, Univ. Michigan Press, Ann Arbor, MI, 1975.
- [23] D. Ha, J. Schmidhuber, Recurrent world models facilitate policy evolution, in: S. Bengio, H. Wallach, H. Larochelle, K. Grauman, N. Cesa-Bianchi, R. Garnett (Eds.), Advances in Neural Information Processing Systems 31, Curran Associates, Inc., 2018, pp. 2455–2467.
- [24] D. Ha, J. Schmidhuber, World Models, arXiv e-prints arXiv:1803.10122 (2018) 1–21.
- [25] S. Nolfi, D. Parisi, J. L. Elman, Learning and Evolution in Neural Networks, Adaptive Behavior 3 (1) (1994) 5–28. doi:10.1177/105971239400300102.
- [26] S. Nolfi, A. Spalanzani, Learning and Evolution: On the Effects of Directional Learning, Artificial Life (2000) 1–16.
- [27] I. Goodfellow, J. Pouget-Abadie, M. Mirza, B. Xu, D. Warde-Farley, S. Ozair, A. Courville, Y. Bengio, Generative Adversarial Nets, in: Z. Ghahramani, M. Welling, C. Cortes, N. D. Lawrence, K. Q. Weinberger (Eds.), Advances in Neural Information Processing Systems 27, Curran Associates, Inc., 2014, pp. 2672–2680.
- [28] A. Radford, L. Metz, S. Chintala, Unsupervised representation learning with deep convolutional generative adversarial networks, arXiv preprint arXiv:1511.06434 (2015) 1–16.
- [29] R. Groß, Y. Gu, W. Li, M. Gauci, Generalizing GANs: A Turing perspective, in: Advances in Neural Information Processing Systems (NIPS), 2017, pp. 6319–6329.
- [30] W. Li, M. Gauci, R. Groß, Turing learning: a metric-free approach to inferring behavior and its application to swarms, Swarm Intelligence 10 (3) (2016) 211–243. doi:10.1007/s11721-016-0126-1.
- [31] R. Der, G. Martius, The playful machine: theoretical foundation and practical realization of self-organizing robots, Vol. 15, Springer Science & Business Media, 2012. doi:10.1007/978-3-642-20253-7.

- [32] G. Martius, J. M. Herrmann, Taming the beast: Guided self-organization of behavior in autonomous robots, in: S. Doncieux, B. Girard, A. Guillot, J. Hallam, J. A. Meyer, J. B. Mouret (Eds.), *From Animals to Animats 11*, Vol. 6226 of LNAI, Springer, 2010, pp. 50–61. doi:10.1007/978-3-642-15193-4_5.
- [33] R. P. Feynman, R. B. Leighton, M. Sands, *The Feynman lectures on physics Vol. 1*, Vol. 1, Basic Books, New York, 2010.
- [34] E. Ising, Beitrag zur Theorie des Ferromagnetismus, *Zeitschrift fur Physik* 31 (1925) 253–258. doi:10.1007/BF02980577.
- [35] H. Hamann, Evolving prediction machines: Collective behaviors based on minimal surprisal, in: *Int. Conf. on Genetic and Evolutionary Computation (GECCO 2014)*, ACM, 2014, pp. 31–32, [extended abstract]. doi:10.1145/2598394.2598507.
- [36] F. Riedo, M. Chevalier, S. Magnenat, F. Mondada, Thymio II, a robot that grows wiser with children, in: *IEEE Workshop on Advanced Robotics and its Social Impacts (ARSO 2013)*, IEEE, 2013, pp. 187–193.